Materials Science and Engineering A 527 (2010) 7252–7260

Contents lists available at ScienceDirect

Materials Science and Engineering A

journal homepage: www.elsevier.com/locate/msea

Hydrogen embrittlement susceptibility of a high strength steel X80

I. Moro[a], L. Briottet[a,*], P. Lemoine[a], E. Andrieu[b], C. Blanc[b], G. Odemer[b]

[a] CEA, LITEN, DTBH, LCTA, F-38054 Grenoble, France
[b] CIRIMAT/ENSIACET, Université de Toulouse, UPS/INPT/CNRS, 4 allée Emile Monso, 31432 Toulouse Cedex 4, France

ARTICLE INFO

Article history:
Received 30 September 2009
Received in revised form 9 July 2010
Accepted 12 July 2010

Keywords:
X80
Hydrogen embrittlement
HELP
HID
AIDE
Hydrogen diffusion

ABSTRACT

The present paper deals with hydrogen embrittlement (HE) susceptibility of a high strength steel grade (X80). The respective implication of different hydrogen populations, i.e. adsorbed, dissolved in interstitial sites, trapped on dislocations and/or microstructural elements on the associated embrittlement mechanisms has been addressed through mechanical testing in high pressure of hydrogen gas at room temperature. Tensile tests at various strain rates and hydrogen pressures have been carried out. Moreover, changes of gas (hydrogen or nitrogen) during loading have been imposed in order to get critical experiments able to discriminate among the potential hydrogen embrittlement mechanisms already proposed in the literature. The results of these tests have shown that hydrogen induces several kind of damages including decohesion along ferrite/pearlite interfaces and microcracks initiations on the specimens external surface. It is shown that decohesion is not critical under the loading paths used in the present study. On the contrary, it appears that the external microcracks initiation, followed by a quasi-cleavage fracture, is responsible for the premature failure of the material in high pressure of hydrogen gas. These experimental results have been further discussed by modeling hydrogen diffusion in order to identify hydrogen populations (adsorbed, diffusible or trapped) involved in HE. It was then demonstrated that adsorbed and near surface diffusible hydrogen are mainly responsible for embrittlement.

1. Introduction

The development of a hydrogen economy would need to set up substructures in order to product, transport, and store hydrogen. The use of pipelines for hydrogen transport seems to be one of the most interesting conveyances as soon as large quantities of hydrogen will have to be provided. In order to reduce the cost of production of pipelines, directly related to the quantity of metal needed, high strength steels are used such as X80 for natural gas. However, previous workers have shown that many high strength steels are susceptible to hydrogen embrittlement, inducing degradations of the mechanical properties [1–3]. The purpose of this study is both to assess the specific resistance of X80 to hydrogen embrittlement and to contribute to an improvement of the understanding of hydrogen effect on high strength steels. Although the hydrogen embrittlement mechanisms are the subject of numerous researches [4–10], it is not clear how to select among them which one is the most active in the present case. In this paper, the mechanical behavior of a high strength steel grade X80 is studied in high pressure of hydrogen gas at room temperature. First, tensile tests have been performed to quantify how much the X80 susceptibility to hydrogen embrittlement is influenced by strain rate and hydrogen pressure. Finally, tensile tests with changes of gas were performed. By correlating the experimental results to hydrogen diffusion simulations, an identification of the hydrogen populations (lattice, trapped or adsorbed) acting predominantly on the degradation of the mechanical properties in hydrogen gas is attempted.

2. Materials and experimental procedures

2.1. Materials

The material of the study was a high strength steel grade X80 which chemical composition was given in Table 1. It was received as pieces of a pipeline (diameter 914 mm, thickness 11 mm) and samples were machined far from the seam-welded zone. From a metallurgical point of view, the material exhibited a ferritic–pearlitic microstructure with a ferrite grain size ranging between 5 μm and 15 μm (Fig. 1a) and with less than 15% of pearlite. A strong microstructural anisotropy was observed due to steel rolling inducing bands of pearlite phases parallel to the circumferential direction of the pipes (Fig. 1b) and elongated along the rolling direction. Smooth and notched axisymmetric tensile specimens were machined in order to locate the loading axis parallel to these bands, i.e. along the longitudinal direction of the pipeline.

* Corresponding author. Tel.: +33 438783315; fax: +33 438785891.
E-mail addresses: isabelle.moro@cea.fr (I. Moro), laurent.briottet@cea.fr (L. Briottet), patrick.lemoine@cea.fr (P. Lemoine), eric.andrieu@ensiacet.fr (E. Andrieu), christine.blanc@ensiacet.fr (C. Blanc), gregory.odemer@ensiacet.fr (G. Odemer).

0921-5093/$ – see front matter © 2010 Elsevier B.V. All rights reserved.
doi:10.1016/j.msea.2010.07.027

Table 1
Chemical composition of X80 (wt.%).

C	Mn	Si	Nb	V	Cu	P	S	Fe
0.075	1.86	0.35	0.05	<0.01	0.22	0.015	<0.003	Balance

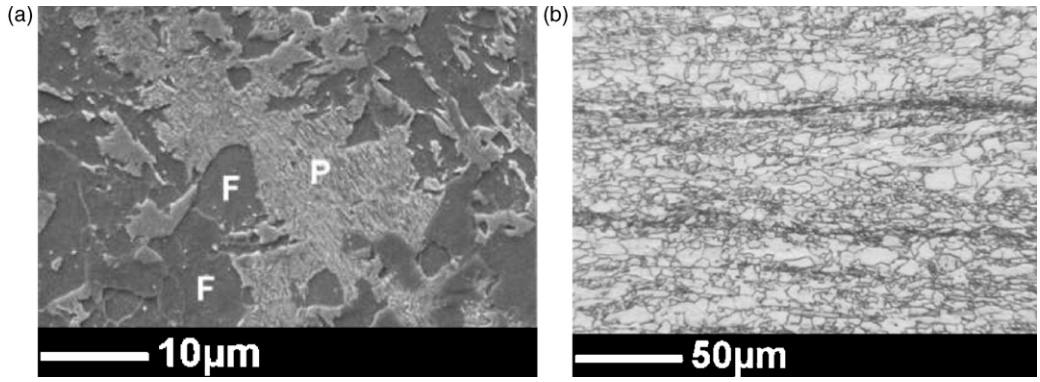

Fig. 1. Ferritic–pearlitic microstructure of X80 (a) with bands of pearlite along the thickness of the pipeline (b).

Before being tested, all the specimens were mechanically polished with a 1200 grade SiC paper to clean the sample surface and to generate similar roughness.

2.2. Tensile tests in gaseous atmosphere

Two specimen geometries were used: smooth axisymmetric specimens, with a gage length of 30 mm and a 6 mm diameter, and notched axisymmetric specimens with a notch radius equal to 10 mm and a stress triaxiality equal to 0.5 according to Bridgman description (Fig. 2). This geometry was chosen to localize rupture in hydrogen gas without changing the HE mechanisms by comparison to smooth specimen [11]. Tensile tests were carried out at room temperature on a MTS servo hydraulic testing system in a pressure vessel filled in hydrogen or nitrogen gas. Load is measured from a load cell located outside of the pressure vessel, corrected from the pressure existing inside. Strains are measured with a clip-on extensometer inside the pressure vessel. Whatever the tests, before applying the mechanical loading, the specimens were exposed in nitrogen gas during 1 h to clean the atmosphere of the pressure vessel from oxygen, and then the vacuum was created. Although residual impurities in the pressure vessel were not measured, this protocol was systematically applied before each tests to ensure a better reproducibility of the vessel atmosphere.

A first set of tensile tests was performed by exposing smooth axisymmetric specimens at 30 MPa either in nitrogen or in hydrogen gas, and with a strain rate of 5×10^{-5} s^{-1}. For the experiments performed in nitrogen atmosphere, the samples were immediately loaded after the cleaning step previously described while, for those performed in hydrogen atmosphere, the specimens were precharged in 30 MPa of hydrogen gas during 30 min in order to favor hydrogen diffusion in the samples before starting tensile tests. Thus, it was assumed that the hydrogen uptake during the precharging step was not surface-limited by oxide or residual oxygen in the hydrogen atmosphere: the hydrogen penetration distance during the precharging step is solely characterized by simple diffusion calculations.

A second set of tensile tests was carried out to investigate the influence of hydrogen pressure. Smooth axisymmetric specimens were tested at 5×10^{-5} s^{-1} with a hydrogen pressure ranging from 0.1 MPa up to 30 MPa.

A third set of experiments consisted in performing the same experiments than before in 30 MPa of hydrogen gas with different strain rates ranging from 5.5×10^{-7} s^{-1} to 0.55 s^{-1}. For comparison, an additional test in nitrogen atmosphere was performed with a strain rate equal to 0.55 s^{-1}. Prior to each test carried out in hydrogen gas, a 30 MPa hydrogen precharging step of 30 min was realised.

A fourth set of tensile tests was carried out by using changes of atmospheres on notched axisymmetric specimens with a displacement rate of 0.05 mm/min. Whatever the tests, the change of atmosphere during mechanical loading was applied at the same displacement, corresponding to the onset of rupture under hydrogen (dark cross in Fig. 3a). Several initial and testing conditions were explored in order to study the influence of the various hydrogen populations on the HE susceptibility of the X80. These conditions can be described as follows (Table 2):

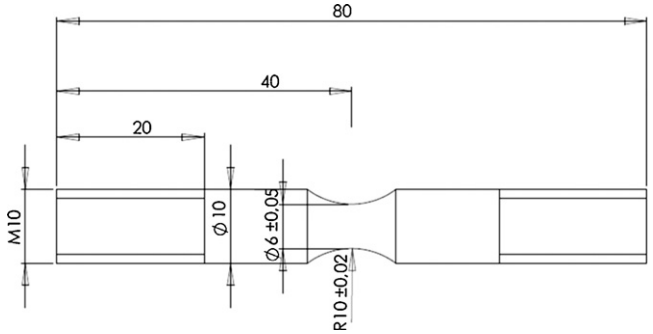

Fig. 2. X80 notched axisymmetric specimen plan.

- For Test 1 (Fig. 3a), referenced as [60 min 30 MPa H_2]/[30 MPa $H_2 \rightarrow$ 0.2 MPa N_2], the sample was first precharged for 60 min in 30 MPa hydrogen. Then, the test was started in 30 MPa of hydrogen gas at 0.05 mm/min and stopped just before estimated failure in hydrogen gas alone. Hydrogen gas was removed and replaced by 0.2 MPa of nitrogen gas in about 8 min. It was assumed that there was no residual hydrogen in the atmosphere after the gas switching from hydrogen to nitrogen. The tensile test was then restarted at 0.05 mm/min until failure. The purpose of this test was to investigate the part of trapped hydrogen on embrittlement. While hydrogen precharging and mechanical loading in hydrogen gas let hydrogen penetrate into the specimen, adsorbed hydrogen (hydrogen present in the firsts atomic layers on the

Table 2
Tests protocols for notched (Tests 1 and 2) and smooth (Test 3) axisymmetric specimens, X refers to the onset of failure in hydrogen gas (dark cross in Fig. 3a).

Test	Specimen	Hydrogen precharging	First gas	Gas switching	Second gas	Test duration in H_2
N_2	Notched	No	30 MPa N_2	No		
H_2	Notched	60 min 30 MPa	30 MPa H_2	No		
Test 1: [60 min 30 MPa H_2]/[30 MPa H_2 → 0.2 MPa N_2]	Notched	60 min 30 MPa	30 MPa H_2	Yes, at X	0.2 MPa N_2	29 min
Test 2: []/[30 MPa N_2 → 30 MPa H_2]	Notched	No	30 MPa N_2	Yes, at X	30 MPa H_2	8 min 35 s
N_2	Smooth	No	30 MPa N_2	No		
H_2	Smooth	30 min 30 MPa	30 MPa H_2	No		
Test 3: [30 min 30 MPa H_2]/[30 MPa N_2]	Smooth	30 min 30 MPa	30 MPa N_2	No		

surface) and near surface diffusible hydrogen desorbed when hydrogen was removed from the atmosphere.

- For Test 2 (Fig. 3a), referenced as []/[30 MPa N_2 → 30 MPa H_2], the specimen was not submitted to any hydrogen precharging before the mechanical loading. It was loaded in 30 MPa of nitrogen gas till failure displacement in hydrogen gas (dark cross in Fig. 3a). Then nitrogen gas was replaced by 30 MPa of hydrogen gas and test was continued till specimen failure. This test was designed to study the promptness and the magnitude of hydrogen embrittlement when material was not precharged and since hydrogen was introduced in the atmosphere during mechanical test. Correlated to Test 1, it investigated the contribution of near surface diffusible and adsorbed hydrogen on embrittlement.

Finally, a tensile test called Test 3 (Fig. 3b) and referenced as [30 min 30 MPa H_2]/[30 MPa N_2], was carried out to investigate the influence of the hydrogen precharging step on the hydrogen embrittlement. A smooth axisymmetric specimen was precharged in 30 MPa of hydrogen gas during 30 min. Then the mechanical loading was carried out in nitrogen gas at 5×10^{-5} s^{-1}.

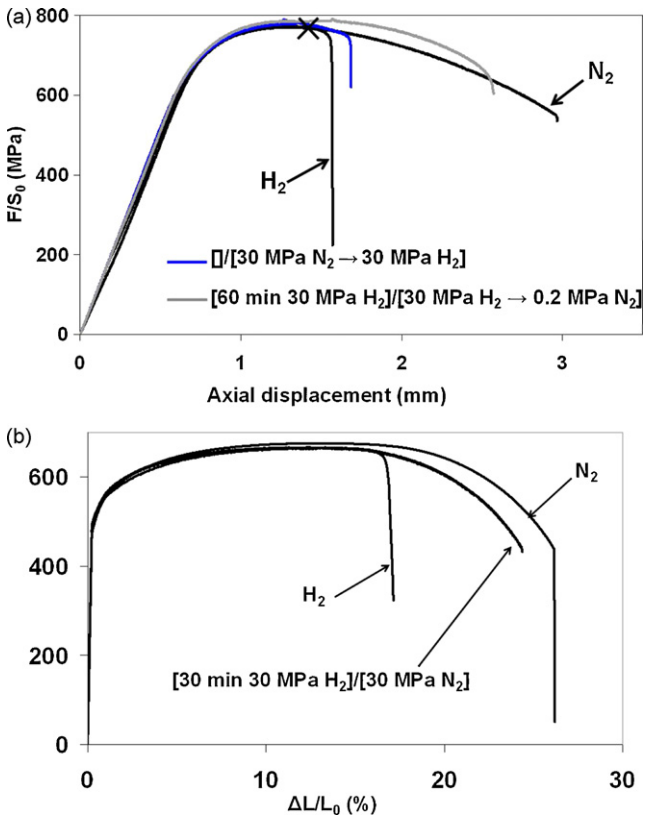

Fig. 3. Interrupted tests on notched axisymmetric specimens (ρ = 10 mm) (a) and on smooth axisymmetric specimens (b).

3. Experimental results

3.1. Hydrogen embrittlement susceptibility of X80

For the first set of experiments, tensile tests on smooth specimens were carried out in 30 MPa of hydrogen (H_2 test) or nitrogen (N_2 test) gas at a strain rate equal to 5×10^{-5} s^{-1}. Each experiment was performed twice and the results were reproducible. Fig. 4 showed representative results underlining that hydrogen had no effect on the yield stress nor on the ultimate tensile stress of the steel as well as on the strain hardening step preceding necking. On the contrary, the strain to failure was strongly reduced which meant that most of the hydrogen effect was concentrated on the last part of the curve.

The corresponding fracture surfaces of the specimens are presented in Fig. 5. Comparison of the fracture surfaces of the specimens tested in nitrogen (Fig. 5a) or hydrogen (Fig. 5c) gas showed that hydrogen reduced significantly necking. Fig. 5a revealed also a strong anisotropy of the surface fracture under nitrogen atmosphere, related to the X80 microstructure anisotropy. To quantify the influence of hydrogen, an embrittlement index E_I was defined according to Eq. (1) where $R_A^{N_2}$ and $R_A^{H_2}$ respectively represented the reduction of area in nitrogen or hydrogen gas.

$$E_I\,(\%) = \frac{R_A^{N_2} - R_A^{H_2}}{R_A^{N_2}} \times 100 \qquad (1)$$

For the H_2 test, the embrittlement index was equal to 68%. These results were well correlated with those of Trasatti et al. [1] who performed tensile tests on X80 axisymmetric notched specimens under continuously hydrogen charging conditions (synthetic seawater at −1000 mV or in 1 N H_2SO_4 at −5 mA/cm^2, both at 22 °C). The authors showed that the main effect of hydrogen was to reduce the necking of specimens and the displacement to failure while the maximum load was not affected by hydrogen charging.

Moreover, Fig. 5a and c showed delamination on the fracture surfaces, but hydrogen enhanced this type of damage. Dealing with the fracture mode, Fig. 5b and d logically showed a ductile fracture with dimples in nitrogen gas (Fig. 5b) and a quasi-cleavage frac-

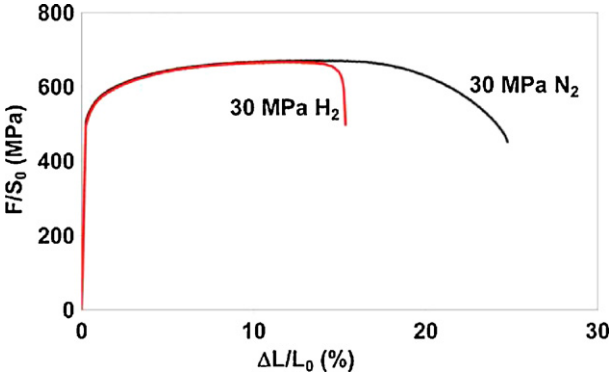

Fig. 4. Influence of hydrogen on the mechanical properties of X80.

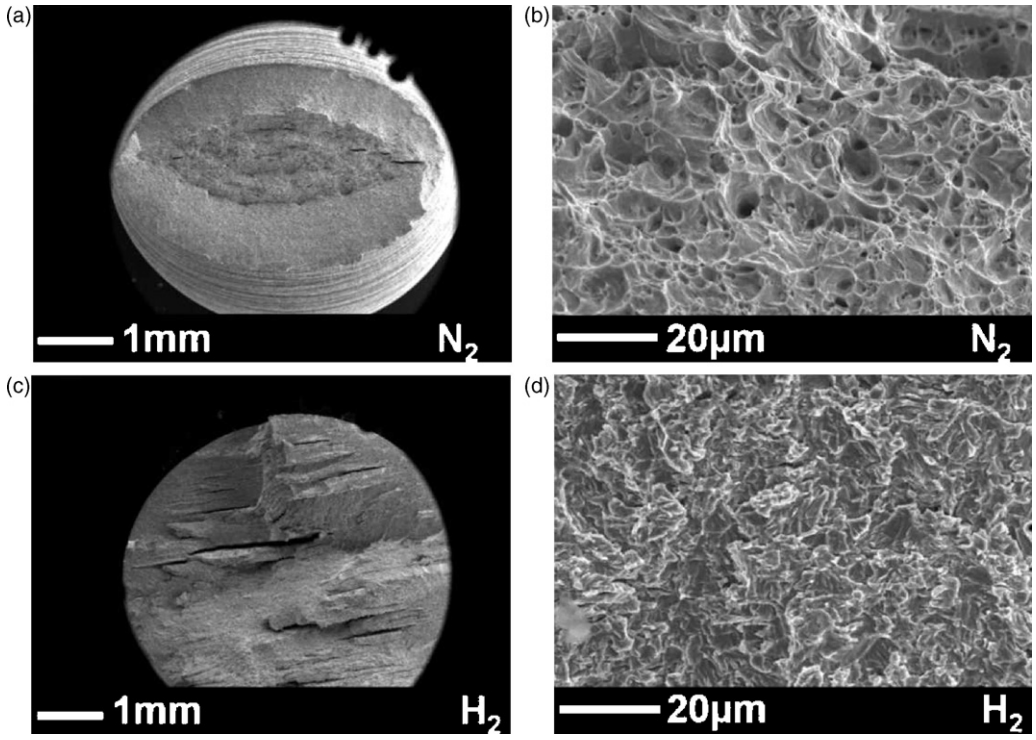

Fig. 5. Fracture surfaces of specimens tested in nitrogen (a and b) and in hydrogen (c and d).

ture mode in hydrogen gas (Fig. 5d). In addition, examination of the gage length external surface of the specimens loaded in hydrogen gas showed circumferential cracks rather homogeneously distributed.

All these features tended to prove that hydrogen induced two main damage modes. The first one, located in the bulk of the specimens, occurred by decohesion at the interface between pearlite alignments and ferrite matrix, easily visible on the fracture surface of the samples loaded in hydrogen gas (Fig. 5c). The second one, located at the surface of the specimen, consisted in brittle circumferential cracks, perpendicular to the loading direction (Fig. 6).

3.2. Influence of hydrogen pressure

The influence of hydrogen pressure was addressed on tensile tests performed at 5×10^{-5} s^{-1}. Four hydrogen gas pressures were investigated (Fig. 7). It was observed that hydrogen induced a similar reduction of strain to failure and necking when hydrogen pressure ranged between 5 MPa and 30 MPa. At 0.1 MPa, *post mortem* analysis, in terms of reduction of area and fracture surface appearance, did not reveal any effect of hydrogen (Table 3). However, a weak decrease of strain to failure indicated the beginning of hydrogen embrittlement. According to Sievert's law and to Langmuir's isotherm, an increase of hydrogen pressure might lead respectively to an increase of hydrogen solubility and of surface-coverage, favoring hydrogen embrittlement. It was worth noticing that, in the present case, these effects were not observed when the pressure was higher than 5 MPa. The critical pressure, which was clearly ranged between 0.1 MPa and 5 MPa, was not determined here.

Table 3
Evolution of delamination and embrittlement index with hydrogen pressure.

Hydrogen pressure	Delamination	E_I (%)
0.1 MPa	No	0
5 MPa	Yes	41
10 MPa	Yes	67
30 MPa	Yes	68

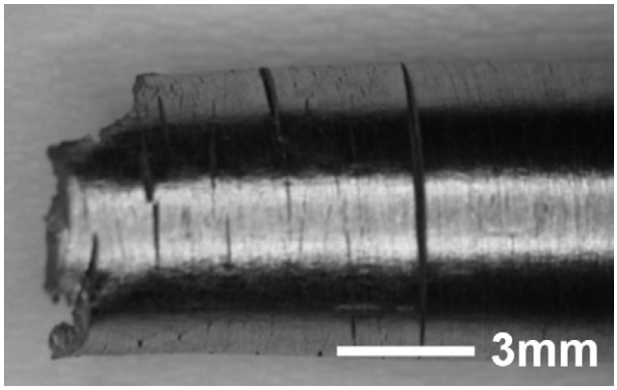

Fig. 6. External cracks at the surface of tensile specimens broken in 30 MPa hydrogen.

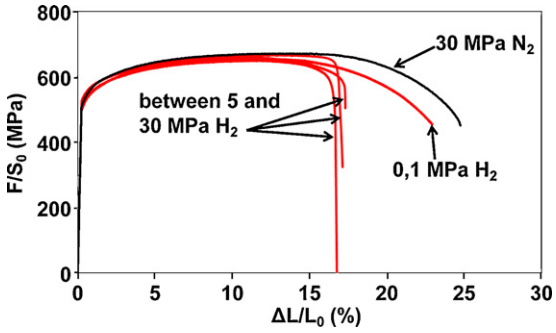

Fig. 7. Tensile tests in hydrogen gas at 5×10^{-5} s^{-1} – effect of hydrogen pressure.

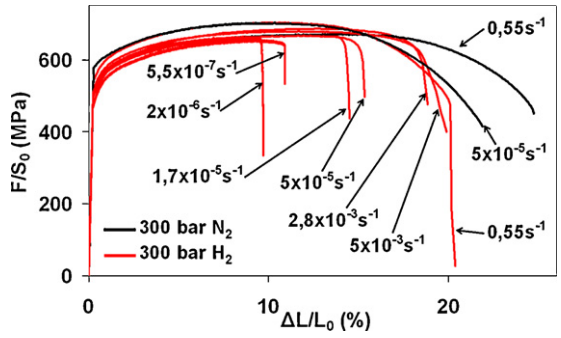

Fig. 8. Influence of strain rate on hydrogen embrittlement of X80. The tensile tests in nitrogen gas are given for comparison.

3.3. Influence of strain rate on HE of X80

The tensile curves obtained for tests performed under hydrogen, as described in the experimental section, are shown in Fig. 8. The strain rates covered six orders of magnitude so that the duration of the tensile tests ranged from 63 h to 0.46 s for strain rates equal to $5 \times 10^{-7}\ s^{-1}$ and $0.55\ s^{-1}$ respectively (Table 4). As said previously, for comparison, two specimens were tested in 30 MPa of nitrogen gas at $5 \times 10^{-5}\ s^{-1}$ and $0.55\ s^{-1}$. Under these latter experimental testing conditions, the material exhibited a weak increase of the yield and ultimate tensile stresses as the strain rate increases while the strain to failure was higher when the specimen was tested at $5 \times 10^{-5}\ s^{-1}$. The reduction of area was nevertheless similar for both specimens leading to a value of 69%.

From a global point of view, the shape of the tensile curves obtained under hydrogen atmosphere was similar for all the strain rates tested. Fig. 8 confirmed again that hydrogen did not influence significantly the yield stress or the ultimate tensile stress but it did reduce the strain to failure. This behavior was clearly visible when comparing results obtained for strain rates equal to $5 \times 10^{-5}\ s^{-1}$ and $0.55\ s^{-1}$ in nitrogen and hydrogen atmospheres. Moreover, it was observed that the strain to failure increased with the strain rate. At high strain rate, i.e. $0.55\ s^{-1}$, strains to failure in nitrogen and hydrogen gas seemed to be nearly similar while at low strain rate, i.e. $5.5 \times 10^{-5}\ s^{-1}$, the strain to failure was half lower in hydrogen than in nitrogen gas. Table 4 showed that the embrittlement index E_I was not influenced by the strain rate over a large range with values around 65%. However, for a high strain rate, i.e. $0.55\ s^{-1}$, E_I dropped from 68% to 20%, still indicating a weak hydrogen embrittlement. SEM observations confirmed the hydrogen effect for such a high strain rate since the fracture surfaces of the corresponding specimens (Fig. 9) exhibited a 350 μm large brittle external ring (area 1 in Fig. 9) while the rest of the fracture surface was ductile (area 2 in Fig. 9). This brittle ring covered roughly 10% of the total fracture surface. Moreover, Fig. 9 revealed a weak delamination for this strain rate which was also observed for the lowest strain rate equal to $5 \times 10^{-7}\ s^{-1}$ (Table 4). For intermediate strain rates, delamination was clearly visible on the fracture surfaces of the corresponding specimens (Table 4).

3.4. Tensile tests with changes of atmosphere

To have a better understanding of the respective contribution of the different populations of hydrogen (i.e. lattice, trapped, adsorbed), three different tensile tests with prompt modifications of the gas were performed on X80 axisymmetric notched specimens as previously described in Table 2.

Fig. 3a and b showed the tensile curves obtained for the three different tests taking into account that, for each condition, experiments were reproducible so that representative results were given

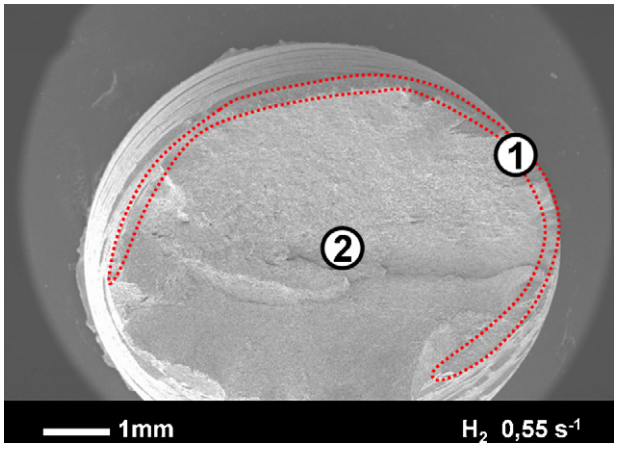

Fig. 9. Fracture surface of an X80 tensile specimen tested in 30 MPa of hydrogen at $0.55\ s^{-1}$.

here. Table 5 summed up the results obtained concerning the embrittlement index and the two main damage modes previously identified, i.e. the presence of external cracks and delamination. It was worth noticing that the embrittlement index calculated following relation (1) could be applied to a notched specimen in order to compare the hydrogen embrittlement susceptibility in different environmental or testing conditions but only for specimens with the same geometry. For comparison, tensile tests on notched axisymmetric specimens were carried out at 0.05 mm/min in 30 MPa of hydrogen or nitrogen gas. All the results of tensile tests with changes of atmosphere are reported both in Fig. 3 and in Table 5 while the corresponding fracture surfaces were shown in Fig. 10. For Test 1 ([60 min 30 MPa H_2]/[30 MPa $H_2 \rightarrow$ 0.2 MPa N_2]) and Test 3 ([30 min 30 MPa H_2]/[30 MPa N_2]), the displacements or elongation to failure were greater than those obtained with specimens tested in hydrogen gas. However, they still remained a bit lower than those obtained with the specimens tested in nitrogen. On the contrary, Test 2 ([]/[30 MPa $N_2 \rightarrow$ 30 MPa H_2]) led to a displacement to failure similar to that observed for specimens tested in hydrogen gas. Calculation of the hydrogen embrittlement index led to an E_I value around 60% for Test 2, which was rather close to the value calculated for H_2 test, while Test 1 led to a highly weaker but meaningful embrittlement index and the value of E_I for Test 3 was too low to conclude for hydrogen embrittlement. However, in spite of the differences observed on the tensile curves for the three different tests with changes of atmosphere, Table 5 also showed that the corresponding specimens exhibited similar damage with both damage modes, i.e. the presence of external cracks and delamination as confirmed by Fig. 10 in which SEM observations of the fracture surfaces are given.

4. Discussion

4.1. Hydrogen adsorption and absorption

Results presented in the previous section revealed a strong susceptibility to hydrogen embrittlement of the X80 steel. To understand the mechanisms explaining the damages observed, it was first necessary to analyze the influence of the precharging step in term of hydrogen absorption. Indeed, it might be assumed that the specimen surface was covered by an oxide layer thick enough to avoid hydrogen adsorption in the specimen during the precharging step. This oxide layer would be mechanically broken during the mechanical loading allowing hydrogen adsorption. However, for tests at high strain rates corresponding to a very short tensile test duration, hydrogen absorption would be compromised. Based

Table 4
Evolution of tests duration, delamination and embrittlement index with strain rate.

Strain rate (s^{-1})	Test duration	External cracks	Delamination	E_I (%)
5.5×10^{-7}	63 h	Yes	Weak	65
2×10^{-6}	21 h 14 min	Yes	Yes	68
1.7×10^{-5}	2 h 45 min	Yes	Yes	67
5×10^{-5}	58 min	Yes	Yes	68
2.8×10^{-3}	129 s	Yes	Yes	66
5×10^{-3}	40 s	Yes	Yes	63
0.55	0.46 s	Yes	Weak	20

on the mechanical response of Test 3 ([30 min 30 MPa H_2]/[30 MPa N_2]), revealing a lower displacement to failure compared to N_2 test (Table 5), and on its fracture appearance, exhibiting delamination, it was concluded that the precharging step obviously induced hydrogen absorption in the specimen. Thus, hydrogen absorption was not fully stopped by the oxide layer covering the specimen surface.

Taking into account this conclusion, the influence of the hydrogen precharging step on embrittlement was discussed.

4.2. Influence of the hydrogen precharging step

To address the hydrogen precharging influence, several tests are discussed below. Test 3 exhibited an E_I value of 5% although the specimen spent 80 min in nitrogen gas between the end of the precharging step and sample failure. Supposing that precharged hydrogen was mainly responsible for embrittlement, this low but non-zero value of E_I was then explained by diffusible hydrogen egress during loading in nitrogen gas (80 min).

Following this assumption, for the tensile test in 30 MPa of hydrogen gas at 0.55 s^{-1}, the embrittlement value of 20% (Table 4) was explained by the precharging step. Indeed, diffusion had no time to occur during the mechanical loading (duration of 0.46 s). However, precharged hydrogen could not be responsible for the strong embrittlement observed for the tensile test performed in hydrogen gas at 5×10^{-3} s^{-1} (E_I = 63%). In this case, the mechanical loading lasted 40 s and, as for the 0.55 s^{-1} tensile test, diffusion had no time to occur. Thus, if the precharging step was predominantly responsible for embrittlement, an E_I value close to 20% should be found, instead of 63%.

Even if Test 3 clearly evidenced that the hydrogen precharging step induced embrittlement, mainly expressed by delamination, tensile tests in hydrogen gas at 0.55 s^{-1} and 5×10^{-3} s^{-1} demonstrated that it was not responsible for the major part of embrittlement under hydrogen gas. This conclusion was reinforced by Test 2. Although this sample was not hydrogen precharged, and lasted in hydrogen gas during only 8 min, it exhibited a strong embrittlement (E_I = 60%).

4.3. Delamination mechanism: hydrogen supersaturation at microstructure interfaces

It was now assumed that hydrogen was present in the material due, at least, to its absorption during the precharging step. This analysis was consistent with the observation in Fig. 9 of a brittle ring on the H_2-precharged specimen strained at 0.55 s^{-1} under hydrogen. Nevertheless, the susceptibility of this specimen to delamination was drastically reduced which was also the case for the specimen tested at very low strain rates (5.5×10^{-7} s^{-1}) for which the duration of the tensile test obviously allowed hydrogen absorption.

Thus, results showed that two main mechanisms competed with one another, i.e. delamination and surface crack initiation and propagation. Concerning the delamination, the results seemed to indicate that the interface between pearlite and ferrite was embrittled due to a local hydrogen supersaturation related to hydrogen transport by dislocations. Delamination was then revealed by the interfacial stresses generated by dislocations pile-up at ferrite/pearlite interfaces. Thus, by decreasing the local material cohesive energy, as proposed in the HID mechanism, hydrogen promoted the material decohesion along these interfaces. At intermediate strain rates ranging from 2×10^{-6} s^{-1} to 5×10^{-3} s^{-1}, the hydrogen flux arriving at ferrite/pearlite interfaces due to dislocation transport and diffusion was efficient. In this case, interfaces between ferrite and pearlite could be dynamically enriched with hydrogen and decohesion favored. On the contrary, at high strain rate, dislocations moved too fast to draw Cottrell atmospheres and, moreover, diffusion did not have sufficient time to occur. Thus, only a little hydrogen was trapped at the pearlite/ferrite interfaces and decohesion was not favored. At sufficient low strain rate, even if hydrogen diffused through the material and was transported by dislocations, it could be assumed that hydrogen had enough time to escape from interfaces which could prevent them from supersaturation. In this case too, delamination was reduced. This supersaturation mechanism may also explain the results of Test 3 evidencing that delamination does not need hydrogen external atmosphere to occur. During the precharging step of the Test 3 sample, hydrogen absorbed and diffused through the material. Once the precharging step ended and the mechanical loading in nitrogen gas started, mobile dislocations trapped lattice hydrogen atoms and brought them to ferrite/pearlite interfaces, thus inducing delamination. Hydrogen transport by dislocations as well as hydrogen supersaturation leading to decohesion are not universally accepted mechanisms. It is thus needed to discuss these two points in the context of this study.

The effect of enhanced diffusion with plastic strain has been addressed by several authors and the results are inconclusive. Ladna et al. [12] performed post-mortem SIMS deuterium measurements on cathodically charged during plastic deformation

Table 5
Results of interrupted tests – E_I: embrittlement index and delamination. D_F: displacement to failure (notched specimens); ε_F: strain to failure (smooth specimens).

Test	D_F (mm)	ε_F (%)	External cracks	Delamination	E_I (%)
N_2 (notched specimen)	3		No	No	
H_2 (notched specimen)	1.6		Yes	Yes	68
Test 1 (notched specimen): [60 min 30 MPa H_2]/[30 MPa H_2 → 0.2 MPa N_2]	2.6		Yes	Yes	25
Test 2 (notched specimen): []/[30 MPa N_2 → 30 MPa H_2]	1.7		Yes	Yes	60
N_2 (smooth specimen)		26	No	No	
H_2 (smooth specimen)		16.8	Yes	Yes	68
Test 3 (smooth specimen): [30 min 30 MPa H_2]/[30 MPa N_2]		24.3	Yes	Yes	5

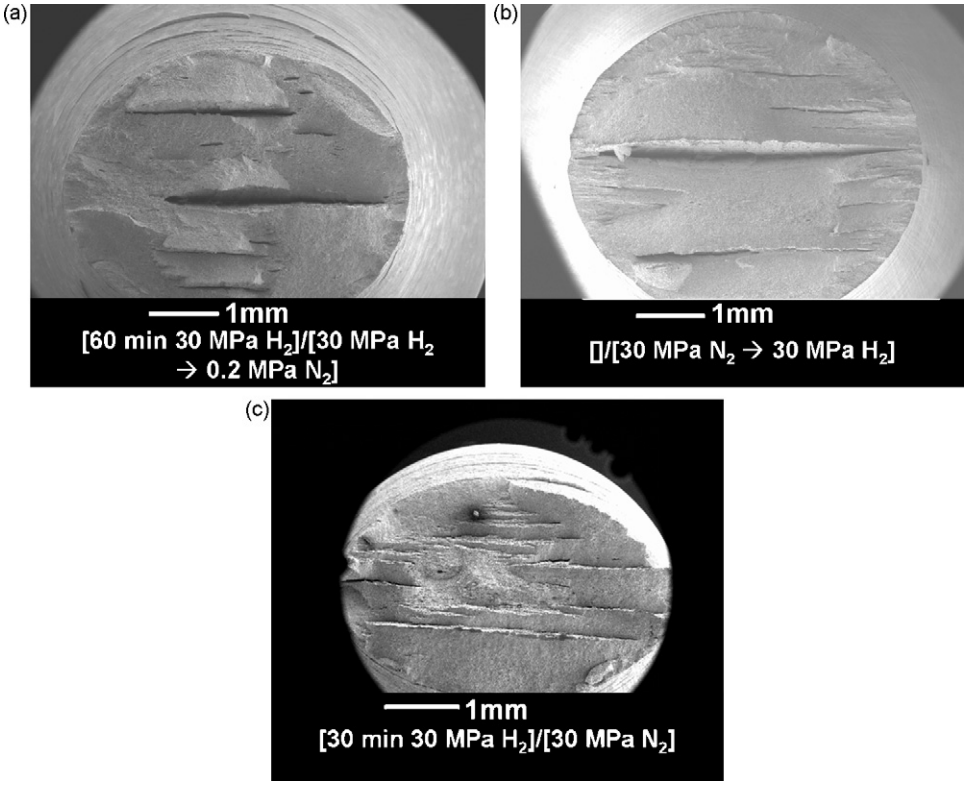

Fig. 10. Fractographies of specimens tested with protocols [60 min 30 MPa H_2]/[30 MPa H_2 → 0.2 MPa N_2] (a), []/[30 MPa N_2 → 30 MPa H_2] (b) and [30 min 30 MPa H_2]/[30 MPa N_2] (c).

specimens in austenitic stainless steels (304S, 310S) and nickel. Although the authors found no evidence of hydrogen transport by dislocations, their results are not transposable to the present material. Indeed, Ladna et al. observed nickel hydrides formation during hydrogen electrochemical charging, and stress induced martensite formation during mechanical loading of 304S steel. By contrast, in the X80 steel, no hydrides were formed and no phase transformation occurred. In 310S steel, Ladna et al. did not observe any difference between SIMS profiles for hydrogen charged specimens with or without straining. However, this result contradicts with previous study [13] on X80 steel in 30 MPa of hydrogen gas at room temperature. It was shown that hydrogen content was greater in specimens mechanically loaded in hydrogen gas compared to hydrogen charged but not strained specimens. These reproducible results also showed that hydrogen content in the material continuously increased with plastic strain. Even if these results did not provide direct evidence that hydrogen can be transported from an external hydrogen atmosphere into the specimen, they clearly demonstrated that dislocations do interact with hydrogen in X80 steel, which was not the case in Ladna et al. study. Moreover, Chene and Brass [14] and Donovan [15] obtained strong evidences for hydrogen accelerated transport by dislocations in Ni base superalloy, iron and stainless steel 304L.

In the present study, it is proposed to explain the disappearance of delamination at high and low strain rates by a hydrogen supersaturation mechanism. Such supersaturation cannot be obtained by diffusion but rather by transport from dislocations piles-up to ferrite/pearlite interface. It is not assumed here that there is a net flux of hydrogen into the specimen from an external hydrogen atmosphere, but it is assumed that hydrogen introduced during the precharging step and the mechanical loading can interact with the dislocations.

Considering hydrogen supersaturation at interfaces, Tien et al. [16] proposed a model for hydrogen transport by dislocations inducing supersaturation through stripping of the solutes off the moving dislocations. The damaging process considered here is then based on the nucleation of hydrogen bubbles at high pressures. Using different assumptions, Hirth [17] and Hirth and Johnson [18] also addressed this problem but considering a trap free matrix. When hydrogen-laden dislocations reach random dislocations annihilation sites, a local hydrogen enrichment is obtained. The difference between this hydrogen arrival rate, and the departure rate by diffusion, governs the local hydrogen supersaturation. The authors calculated that the hydrogen concentration reached by this mechanism is too small to create pressurized voids that can initiate hydrogen embrittlement in the alloy. Reinvestigating the above models, Nair et al. [19] considered that depending on the initial assumptions (trap–no trap) a significant local hydrogen enrichment can finally occur at interfaces in both ferritic and austenitic steels. Back to our experimental results, dimples initiated by hydrogen bubbles were not observed at the ferrite/pearlite interfaces. To explain the observed strain rate influence, it was proposed in this paper that a local hydrogen supersaturation might occur at these interfaces and induced decohesion, such as in the HID mechanism, instead of pressurized voids. In this case, the supersaturation did not need to be excessive.

Finally, in the present case, even if delamination was observed, it was not critical under the loading paths used in the present study, i.e. it did not induce a material premature failure. However, this damage could be critical for loading directions out of the pearlite planes.

4.4. Hydrogen population involved in external cracks initiation and propagation

As said previously, it was necessary to take into account two main mechanisms, delamination and surface cracks initiation and propagation. Indeed, it was worth noticing that delamination

was observed as well as cleavage fracture of the ferrite that resulted from the propagation of the external circumferential cracks observed on the specimen. Contrary to delamination, this latter damage was observed whatever the strain rates (Table 4), demonstrating that it was not induced by hydrogen transport by dislocations but by adsorbed or near surface diffusible hydrogen. Observation of a brittle ring on the sample tested at 0.55 s^{-1} (Fig. 9) showed that crack initiation easily occurred even at high strain rates. This could be related to a high hydrogen concentration in the first layers of the samples. A question arises: what was the hydrogen effect and what hydrogen populations were implied in the cracks propagation and then how the effect of the strain rate could be explained? Tests performed with changes of atmosphere and comparison of tensile tests in hydrogen gas at various strain rates could bring experimental evidences to answer to these questions.

First, the sample submitted to Test 1 did not exhibit a significant reduction of elongation to failure even if external cracks were observed due to the exposition to hydrogen atmosphere during the precharging step and the first part of the tensile test (Fig. 3a). Thus, in nitrogen gas, the specimen failure is not mainly controlled by these external cracks previously initiated in hydrogen gas: the E_I value increases from 25% for Test 1 to 68% for H_2 test. Thus, the presence of external hydrogen on the crack surface is responsible for their easier propagation.

Test 1 also evidenced the reversibility of hydrogen embrittlement stressed by the fact that, once hydrogen gas was removed from the external atmosphere, embrittlement strongly decreased. Indeed, the displacement to failure of Test 1 (2.6 mm) was greater than the H_2 test (1.6 mm) and its E_I value (25%), although significant, was almost 3 times lower than the H_2 test (68%). To complete this investigation, a tensile test greatly similar to the Test 1 was carried out. However, just after the change of external atmosphere from hydrogen to nitrogen gas, a dwell of 3 h in nitrogen gas was realized before the mechanical loading was continued in nitrogen gas till specimen failure. This test exhibited an E_I value of 19% and *post mortem* analyses evidenced several external cracks. Because during the 3 h in nitrogen gas hydrogen diffused and desorbed from the sample, it was then concluded that the E_I value of both this last test and Test 1 were mainly due to damages previously initiated in hydrogen gas rather than by a remaining hydrogen. Thus, hydrogen embrittlement is reversible once hydrogen is removed from the external atmosphere.

Second, the experimental result of Test 1 correlated to the simulation of hydrogen diffusion was used to show that trapped hydrogen was not involved in crack propagation.

CAST3M FEM calculations were carried out to simulate the hydrogen diffusion coupled with the mechanical fields. Simulations were performed on the basis of the model developed by Krom et al. [20,21] and assuming an equilibrium between hydrogen in lattice sites and traps [22]. The values of the model parameters were chosen as: trap binding energy $W_b = 40$ kJ/mol, number of lattice sites $N_L = 5.1 \times 10^{+29}$ m^{-3}, lattice diffusion constant $D_0 = 1.27 \times 10^{-8}$ m^2 s^{-1}, partial molar volume of hydrogen $V_H = 2 \times 10^{-6}$ m^3/mol. These parameters were chosen in agreement with previous works [20,21] and were well adapted to diffusion in pure iron. In a ferritic steel, the chosen trap binding energy physically corresponded to rather deep traps, such as screw, edge or mixed dislocations cores, to grain boundaries and to vacancies. Indeed, previous studies have shown that their W_b values are estimated to 40 kJ/mol or more [22–26]. Thus, the conclusions obtained in the following for 40 kJ/mol will be applicable for higher energy traps. The influence of plastic deformation on trapped hydrogen concentration (function $C_T(\varepsilon_p)$ Eq. (2)), has been established by measuring the hydrogen concentration in plastically deformed X80 and has already been presented elsewhere [27]. With the few assumptions presented elsewhere [27] considering one site per

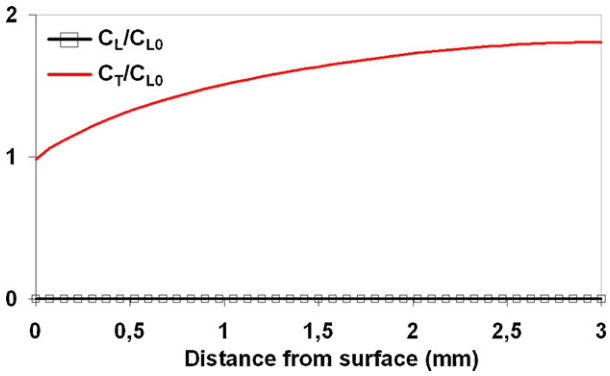

Fig. 11. Evolution of lattice (C_L) and trapped (C_T, $W_b = 40$ kJ/mol) hydrogen concentration along the smallest radius of the specimen in the initial configuration just before loading in nitrogen environment – [60 min 30 MPa H_2]/[30 MPa H_2 → 0.2 MPa N_2] test.

traps and Oriani's equilibrium, this equation can be directly related to the trap density which also evolved with plastic strain.

$$C_T\left(\frac{at_H}{m^3}\right) = 10^{24.73-3.74\exp(-60.17\varepsilon_p)} \quad (2)$$

The simulation of Test 1 was realized. It started along with exposure of the specimen to 30 MPa hydrogen during 60 min. A lattice hydrogen concentration C_{L0}, equal to 4.4×10^{-3} weight ppm (according to Sievert's law at room temperature in 30 MPa of hydrogen gas), was imposed on the external surface of the specimen. It was assumed that the initial hydrogen concentration in the material was equal to zero. This simulation did not take into consideration hydrogen adsorption, whose kinetic was unknown, nor the heterogeneous microstructure of the material. Fig. 11 displays the evolution of trapped and lattice hydrogen in the material along the smallest radius of the specimen, in the initial configuration, and just before the tensile test is started again in nitrogen gas (dark cross in Fig. 3). Lattice hydrogen diffused and left the specimen. By contrast, C_T remained high because hydrogen did not have enough time to escape from the considered traps. Because this test exhibited a weak reduction of displacement to failure and a small embrittlement index, and in accordance with a previous work [28], it was concluded that deeply trapped hydrogen ($W_b > 40$ kJ/mol) was not involved in the hydrogen embrittlement mechanisms of X80. Indeed, these results obtained with a trap binding energy value of 40 kJ/mol would still be obtained if the simulations used a greater value of W_b. Thus, only diffusible and/or adsorbed hydrogen may be responsible for the embrittlement.

Third, results of Test 2 and comparison of tensile tests at 0.55 s^{-1} and at 5×10^{-3} s^{-1} demonstrated the significant part of adsorbed and near surface diffusible hydrogen in embrittlement.

Test 2 showed that hydrogen did not need to diffuse deep into the bulk of the material to induce a strong embrittlement. While this sample lasted only 8 min in hydrogen gas (from the moment when nitrogen was removed to the specimen failure in hydrogen), it exhibited a similar embrittlement than the H_2 test (Table 5). Considering usual hydrogen diffusion coefficient in ferritic–pearlitic steels [29], during an 8 min test hydrogen could not diffuse deeper than 50 μm. It was concluded that the major part of embrittlement was due to near surface diffusible hydrogen and/or to adsorbed hydrogen.

Comparison of tensile tests in 30 MPa of hydrogen gas at 0.55 s^{-1} and at 5×10^{-3} s^{-1} was also relevant to confirm this assumption. While the first test lasted 0.46 s and exhibited an E_I value of 20%, the second one lasted 40 s and showed a 3.2 times greater embrittlement ($E_I = 63\%$). In such a short time hydrogen could not diffuse deeper than about 15/20 μm. To conclude, embrittlement was not

due to hydrogen in the bulk of the specimen, but more likely to adsorbed and near surface diffusible hydrogen (in accordance with the AIDE model [6,7]). This could explain the influence of hydrogen pressure on hydrogen embrittlement. Indeed, according to Langmuir's isotherm, pressure modified the specimen surface-coverage. Thus, the saturation of the surface by adsorbed hydrogen induced the observed pressure threshold. However, tensile tests in hydrogen gas at various strain rates demonstrated that embrittlement increased with test duration (Table 4, Fig. 8), which implied a time dependent embrittlement mechanism, such as diffusion. Thus, diffusible hydrogen was probably responsible for the increase of embrittlement at low strain rate, involving mechanisms such as Hydrogen Induce Decohesion (HID) [7] and Hydrogen Enhanced Localized Plasticity (HELP) mechanisms [4,8,9,30–32].

The identification of hydrogen population implied in embrittlement led us to assume that the premature material failure in hydrogen gas comprised three successive steps. First, adsorbed and near surface diffusible hydrogen induced a decrease of the material surface energy. Once the axial stress was greater than a threshold value, external cracks initiated along the gage length. Second, by diffusion process, diffusible hydrogen concentration increased at external crack tips because of the positive and strong hydrostatic stress generated. Thus, by a physical mechanism such as HID or HELP, crack propagated with a fracture mode of quasi-cleavage. Last, once a crack reached a critical length value, which achieved the material toughness, brutal and final failure occurred. To confirm and detail the proposed mechanisms, additional tests including changes of atmosphere at higher velocity (i.e. a few seconds) are under way.

5. Conclusion

Gaseous hydrogen embrittlement of a high strength steel grade X80 steel was studied through tensile tests. It was shown that X80 was susceptible to hydrogen embrittlement at room temperature for hydrogen pressure greater than 0.1 MPa. Embrittlement increased until a pressure of 10 MPa and was roughly constant above this value. The experimental results indicated that hydrogen embrittlement was influenced by both hydrogen pressure and strain rate in accordance with literature [6,11]. In 30 MPa of hydrogen gas, decreasing strain rate resulted in increasing hydrogen embrittlement.

Special tests including prompt modification of the testing atmosphere from hydrogen to nitrogen (or the reverse) during the mechanical tests were performed. The results contributed to a better understanding of the role played by the different hydrogen populations in the observed phenomena. These tests demonstrated that gaseous hydrogen embrittlement was reversible. Correlated to hydrogen diffusion simulation coupled to the mechanical fields, it appeared that three populations were involved at different degrees in hydrogen embrittlement of X80. First, trapped hydrogen at ferrite/pearlite interfaces induced interface decohesion. Although not critical in this study, this mechanism might take importance depending on the loading direction. The noticed reversibility of hydrogen embrittlement implied adsorbed and near surface diffusible hydrogen in agreement with the AIDE model. However, to describe the strain rate influence, diffusible hydrogen should also be considered. Of course, the predominance of one of these mechanisms depended on the experimental parameters.

References

[1] S.P. Trasatti, E. Sivieri, F. Mazza, Mater. Corros. 56 (2005) 111–117.
[2] N. Eliaz, A. Shachar, B. Tal, D. Eliezer, Eng. Fail. Anal. 9 (2002) 167–184.
[3] D. Hardie, E.A. Charles, A.H. Lopez, Corros. Sci. 48 (2006) 4378–4385.
[4] H.K. Birnbaum, P. Sofronis, Mater. Sci. Eng. A176 (1994) 191–202.
[5] H.K. Birnbaum, Scripta Metall. Mater. 31 (1994) 149–153.
[6] S.P. Lynch, Met. Forum 2 (1979) 189–200.
[7] S.P. Lynch, Proceedings NACE International Conference Corrosion 2007, 2007 (paper 07493).
[8] P.J. Ferreira, I.M. Robertson, H.K Birnbaum, Acta Mater 46 (1998) 1749–1757.
[9] D.C. Ahn, P. Sofronis, R.H. Dodds Jr., Int. J. Hydrogen Energy 32 (2007) 3734–3742.
[10] P. Sofronis, Y. Liang, N. Aravas, Eur. J. Mech. A: Solids 20 (2001) 857–872.
[11] D.P. Abraham, C.J. Altstetter, Metall. Mater. Trans. 26A (1995) 2849–2858.
[12] B. Ladna, H.K. Birnbaum, Acta Metall. 35 (1987) 1775–1778.
[13] I. Moro, Ph.D. Thesis, University of Toulouse III, 2009.
[14] J. Chene, A.M. Brass, Scripta Mater. 40 (1999) 537–542.
[15] J.A. Donovan, Metall. Trans. 7A (1976) 1677–1683.
[16] J. Tien, A.W. Thompson, I.M. Bernstein, R.J. Richards, Metall. Trans. 7A (1976) 821–828.
[17] J.P. Hirth, Metall. Mater. Trans. 11A (1980) 861–890.
[18] J.P. Hirth, H.H. Johnson, in: R.A. Latanision, J.R. Pickens (Eds.), Atomistics of Fracture, Plenum Press, New York, 1983, pp. 771–785.
[19] S.V. Nair, R.R. Jensen, J.K. Tien, Metall. Trans. 14A (1983) 385–393.
[20] A.H.M. Krom, R.W.J. Coers, A. Bakker, J. Mech. Phys. Solids 47 (1999) 971–992.
[21] A.H.M. Krom, H.J. Maier, R.W.J. Koers, A. Bakker, Mater. Sci. Eng. A27 (1999) 22–30.
[22] R.A. Oriani, Acta Metall. 18 (1970) 147–157.
[23] A.J. Kumnick, A.H. Johnson, Acta Metall. 28 (1980) 33–39.
[24] G.M. Pressouyre, I.M. Bernstein, Metall. Trans. 9A (1978) 1571–1580.
[25] V. Ekkarut, Ph.D. Thesis, University of Hamburg, 2005.
[26] A.M. Brass, J. Chêne, J. Coudreuse, Technique de l'Ingénieur M176.
[27] I. Moro, L. Briottet, P. Lemoine, E. Andrieu, C. Blanc, G. Odemer, J. Chêne, F. Jambon, Proceedings of the 2008 International Hydrogen Conference on Effects of Hydrogen on Materials, Jackson Lake Lodge, Wyoming, USA, 2008.
[28] L. Coudreuse, P. Neumann, Application des critères de mécanique de la rupture aux matériaux ductiles chargés en hydrogène, Commission Européenne Recherche Technique acier, EUR 17872, 1998.
[29] H.L. Eschbach, F. Gross, S. Sculien, Vacuum 13 (1963) 543–547.
[30] H.K. Birnbaum, I.M. Robertson, P. Sofronis, D. Teter, Eur. Fed. Corros.Publ. 21 (1997) 172–195.
[31] D.G. Ulmer, C.J. Altstetter, Acta Metall. Mater. 39 (26) (1991) 1237–1248.
[32] I.M. Robertson, Eng. Fract. Mech. 68 (2001) 671–692.